*Remote Sens.* **2015**, *7*, 1021-1047; doi:10.3390/rs70101021

OPEN ACCESS

*remote sensing*

**ISSN 2072-4292**

www.mdpi.com/journal/remotesensing

*Article*

# GRACE Gravity Satellite Observations of Terrestrial Water Storage Changes for Drought Characterization in the Arid Land of Northwestern China

**Yanping Cao [1,2], Zhuotong Nan [1,*] and Guodong Cheng [1]**

[1] Cold and Arid Regions Environmental and Engineering Research Institute, Chinese Academy of Sciences, Lanzhou, 730000, China; E-Mails: caoyp@lzb.ac.cn (Y.P.C.); gdcheng@lzb.ac.cn (G.D.C)

[2] University of Chinese Academy of Sciences, Beijing 100049, China

* Author to whom correspondence should be addressed; E-Mail: nztong@lzb.ac.cn; Tel.: +86-931-496-7741.

Academic Editors: Arnon Karnieli, Richard Gloaguen, and Prasad S. Thenkabail

*Received: 11 June 2014 / Accepted: 12 January 2015 / Published: 16 January 2015*

---

**Abstract:** Drought is a complex natural hazard which can have negative effects on agriculture, economy, and human life. In this paper, the primary goal is to explore the application of the Gravity Recovery and Climate Experiment (GRACE) gravity satellite data for the quantitative investigation of the recent drought dynamic over the arid land of northwestern China, a region with scarce hydrological and meteorological observation datasets. The spatiotemporal characteristics of terrestrial water storage changes (TWSC) were first evaluated based on the GRACE satellite data, and then validated against hydrological model simulations and precipitation data. A drought index, the total storage deficit index (TSDI), was derived on the basis of GRACE-recovered TWSC. The spatiotemporal distributions of drought events from 2003 to 2012 in the study region were obtained using the GRACE-derived TSDI. Results derived from TSDI time series indicated that, apart from four short-term (three months) drought events, the study region experienced a severe long-term drought from May 2008 to December 2009. As shown in the spatial distribution of TSDI-derived drought conditions, this long-term drought mainly concentrated in the northwestern area of the entire region, where the terrestrial water storage was in heavy deficit. These drought characteristics, which were detected by TSDI, were consistent with local news reports and other researchers' results. Furthermore, a comparison between TSDI and Standardized Precipitation Index (SPI) implied that GRACE TSDI was a more reliable

integrated drought indicator (monitoring agricultural and hydrological drought) in terms of considering total terrestrial water storages for large regions. The GRACE-derived TSDI can therefore be used to characterize and monitor large-scale droughts in the arid regions, being of special value for areas with scarce observations.

**Keywords:** GRACE gravity satellite; terrestrial water storage; TSDI; drought; arid region

## 1. Introduction

Drought, as a complex natural hazard, develops slowly but can last for months or even years, and possibly causes more serious harm compared with other natural disasters (e.g., earthquakes and floods). Drought seriously damages agricultural production, ecosystems, and economic and social conditions [1]. In recent years, global climate change had a direct effect on the frequency and intensity of extreme drought events in many regions across the world, especially in semi-arid areas such as northwestern China [2]. During the first decade of the 21st century, China suffered from a series of severe droughts [3]. In China, the annual average crop area that suffered from drought was of 62.0 million acres in the beginning of this century, in comparison to 28.7 million acres in the 1950s [4]. The economic losses are also huge. For example, the annual average grain production loss rose to 34.9 million tons in the first decade of the 21st century, a loss which is 703% larger compared to that in the 1950s [4]. Reported direct economic losses from droughts were over 16 billion USD in 2009 in China [5]. In the face of increasingly severe droughts, it is urgent to take effective measures to continuously monitor this phenomenon.

The arid region of northwestern China, located in the hinterland of the Eurasian continent [6], receives scarce annual precipitation. Drought, a major natural disaster in this region, has deep and extensive influences on human society. Due to global warming, extreme precipitation and temperature events occur much more frequently than ever before in this region [7]. Those events make the climate increasingly complex, inducing many more drought disasters. Drought has seriously hindered local economic development and even threatened human lives.

In China, the traditional methods for drought monitoring are based primarily on hydrological and meteorological data. For example, using the Standardized Precipitation Evapotranspiration Index (SPEI) with monthly precipitation and air temperature at over six hundreds sites over China, Yu *et al.* [8] found that extreme droughts occurred more severely and more frequently during the last three decades in western Northwest China, and a significant drying trend was detected over the central and eastern regions of Northwest China. Zhai *et al.* [9] analyzed the frequency of drought occurrence in Gansu Province (32.59°–42.79°N and 92.76°–108.71°E), which is a part of the arid land of northwestern China, in the last 50 years using the Standardized Precipitation Index (SPI), and concluded that short time droughts severely affected urban and rural livelihoods as well as agricultural development. The strengths of these traditional methods lie in their simplicity, as they are based solely on hydrological and meteorological data. However, drought monitoring based on these traditional methods may be inaccurate in some regions that have complex terrain or fewer measuring sites.

With the development of remote sensing technology, the methods to obtain drought information using multi-temporal, multi-angle, and multi-spectral satellite data at regional scales are maturing gradually.

For example, Zhang *et al.* [10] monitored meteorological drought over northern China using multi-sensor microwave remote sensing data, which was validated with the results from different timescale SPIs in northern China, and concluded that microwave remote sensing drought indices performed better for short-term drought monitoring. The Gravity Recovery and Climate Experiment (GRACE) satellite provides new gravity data that can be used to monitor terrestrial water storage changes (TWSC), which is vertically divided into five parts: groundwater, soil moisture, surface water, snow/ice water and biological water storage [11]. Based on the spatiotemporal variations in terrestrial water storage (TWS), drought characterizations can be obtained. This method has been successfully applied in some regions. Yirdaw *et al.* [12] introduced the GRACE-derived total storage deficit index (TSDI) for drought characterization in the Canadian Prairie. Leblanc *et al.* [13] combined GRACE-derived TWSC with *in situ* and modeled hydrological data to present water deficit propagation and increasing droughts of different types in the early 21st century in southeast Australia. Chen *et al.* [14] monitored the extreme drought event in 2005 in the Amazon river basin using the GRACE satellite data. Considering the applications mentioned above, GRACE satellite data has proven resourceful for drought characterization.

As a fact, there are few hydrological and meteorological stations which are unevenly distributed across the arid land of northwestern China. It is therefore hard to accurately monitor the extent of drought using traditional drought monitoring methods. The objective of this paper is to assess the recent droughts over northwest China using the GRACE gravity satellite data. This data was used to recover the TWSC in the study area from 2003 to 2012. The GRACE-derived TWSC was thereafter validated against water storage changes modeled by the hydrological models as well as precipitation observations in the arid region. Based on the GRACE-derived water storage changes, the drought indicator TSDI was calculated and used to characterize the spatiotemporal distribution of drought in northwestern China. GRACE-derived drought results were compared with the news recorded, previous studies, and SPI monitoring results. Our results will provide scientific information for drought monitoring in large but data-scare regions, such as northwest China.

## 2. Data and Methods

### *2.1. Study Area*

The arid land of northwestern China [15] represents a typical arid region of China (see Figure 1). The western and northern edges of the region lie along the national boundaries of China, while the southern edge lies along the border of Xinjiang Uygur Autonomous Region (Xinjiang hereafter) and the eastern edge is bounded by the Helan Mountains. This region covers an area of 2,200,000 $km^2$, extending between the longitudes 73°–108°E and latitudes 34°–50°N. It accounts for 22% of the total area of China, including Xinjiang, the Hexi Corridor region of the Gansu Province (Hexi Corridor hereafter), parts of Ningxia Hui Autonomous Region, and the western part of the Inner Mongolia Autonomous Region.

The study region is located in the center of the Eurasian continent far away from the ocean. It is surrounded by high mountains, and consists of alternating high mountain ranges and dry basins. Generally, desert plains and foothills are found in the south part, moderate-height mountains in the middle, and high mountains in the north [15]. The climate is of a typical continental arid type, with significant westerly winds, little precipitation, and large potential evapotranspiration, leading to an

extensive distribution of Gobi deserts and loess sediment deposits. The local climate varies with the complex topography and geological structure: moving from lower basin to mountain, a significant vertical increment in precipitation has been observed of up to 500 mm of annual precipitation in the Tianshan, the Altai, and the Qilian Mountains. In contrast, the temperature in the basin plains is higher than in the mountains. Precipitation mostly happens in summer, with the exception of some special regions such as the northwestern part, where more precipitation is concentrated in spring and less in winter. Seasonal temperatures are widely varied; the temperature quickly goes up in spring, peaks in summer, rapidly drops down in autumn, and reaches a minimum during winter.

Rich precipitation in the mountains forms runoff, and then is routed into inland rivers and lakes. These bodies provide surface water resources to the region's basin plains. The hydrological cycle system is closed, as there are no surface or subsurface flow connections with any global ocean or other catchment areas. Water is frequently exchanged between surface water, soil moisture, and groundwater in the piedmonts. Meanwhile, rapid population growth in this arid land exacerbates the depletion of water and is harming the fragile local water system.

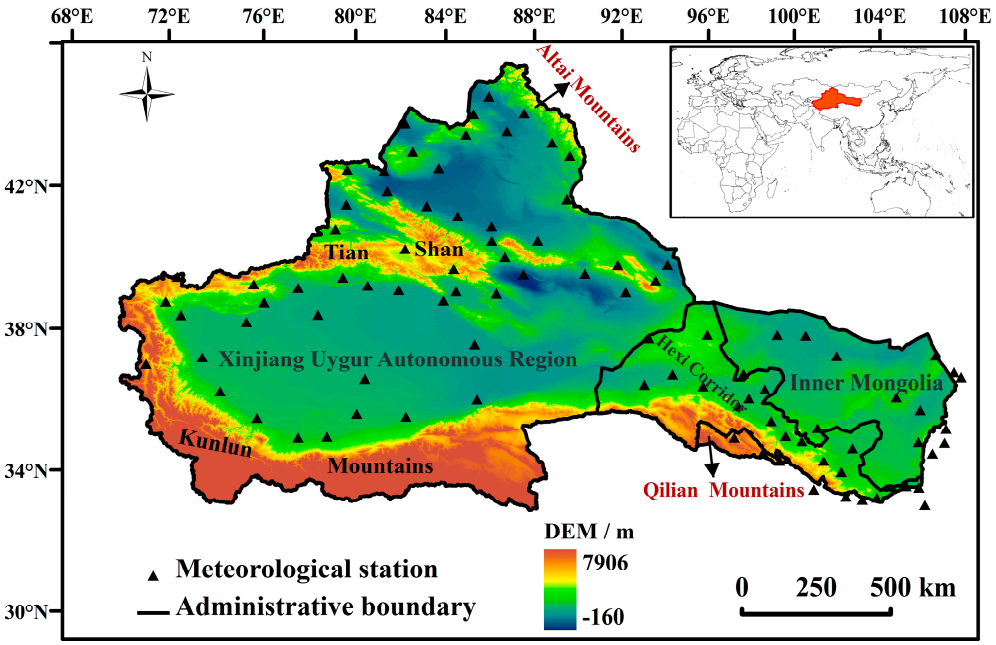


**Figure 1.** Map of the arid land of northwestern China.

### *2.2. GRACE Data*

GRACE Level-2 RL05 data, including time series of spherical harmonic coefficients of the Earth's gravity field, is currently available at three GRACE data processing centers: CSR/UTA (University of Texas at Austin), GFZ/ISDC (Information System and Data Center), and JPL/PO.DAAC (Physical Oceanography Distributed Active Archive Center). RL05 data, with the same signals in RL04, has been improved with significantly noise reduction. This paper uses the GRACE Level-2 RL05 data provided by CSR, which is then truncated to a degree and an order of 90. The data spans from January 2003 to December 2012, with the exceptions of June 2003, January and June 2011, and May and October 2012 due to data loss. Given that the $C_{20}$ coefficient measured by satellite laser ranging (SLR) is much better than that in RL05, $C_{20}$ in RL05 was replaced with SLR $C_{20}$ [16]. Also, due to the reference frame used

in the determination of GRACE satellite gravity field, gravity field coefficients of degree 1 in RL05 were processed as zeros. However, the degree 1 information may have a significant impact on the recovery of surface mass variations. To improve the accuracy and precision in deriving TWSC, the original gravitational coefficients of degree 1 in RL05 were replaced by those calculated by Swenson *et al.* [17]. Monthly time-variable gravity coefficients were calculated by removing the temporal mean of the spherical harmonic coefficients from January 2003 to December 2012. A de-correlation filter [18] was applied to reduce the effects of noisy north-south stripes in the monthly time-variable coefficients. Correlated noises (north-south stripes) were removed from coefficients for orders (m) greater than 15 using a 5th order polynomial, which was fit as a function for each odd or even set for a given order. Then, a fan filter [19] with an averaging radius of 300 km was used to reduce other remaining noises while attempting to maintain the real signal. Subsequently, these processed spherical harmonic coefficients were transformed into gridded data at a 1 by 1 degree spatial resolution, indicating the Earth's surface mass variations, which, in most regions, were mainly caused by the redistribution of water on continents or in oceans. The results were further improved by glacial isostatic adjustment (GIA), which was small in the study region, as per the work of Paulson *et al.* [20]. The mass variations were then converted to TWSC in units of equivalent water height (EWH). The Albers equal area conic projection and WGS 1984 datum were used to project the 1 by 1 degree gridded data, which was then interpolated into a finer resolution of 10 km by 10 km using the Kriging method.

### *2.3. Hydrological Models Data*

To evaluate TWSC measured by GRACE, the results were compared with TWSC from the four hydrological models: three models of the Global Land Data Assimilation System (GLDAS) [21] (Noah, VIC, and Mosaic) and the Climate Prediction Center (CPC) model. These hydrological models have been widely used for global and regional hydrological studies. For example, GLDAS soil moisture, snow water equivalent, and canopy water storage data were jointly used to separate groundwater storage changes from GRACE-derived TWSC [22]. Syed *et al.* [23] estimated global TWSC in major river basins using GLDAS data and compared the results with GRACE-derived TWSC. Based on GLDAS and CPC models data and GRACE derived TWSC, Feng *et al.* [24] evaluated the groundwater depletion in North China. However, GLDAS models did not provide surface water and groundwater storage, while the CPC model could provide soil moisture content but not snow water equivalent. In this paper, we averaged the four versions of TWSC from hydrological models as the best estimate of TWSC. In order to be comparable with GRACE TWSC, model-based monthly TWS were converted to spherical harmonic coefficients with a degree and order of 90 [25]. The exact same data processing procedure was followed as was done with GRACE data. The temporal mean of the study period of January 2003 to December 2012 was computed and the Fan filter with a 300 km radius was applied. Since the hydrological model data had no stripes errors, no de-correlation filter was used for the model data. After the same projection and resampling into 10 km by 10 km resolution was applied, a comparable model-based TWSC dataset was obtained.

There are only a limited number of hydrological and meteorological sites in the large study region, which are insufficient to verify GRACE results. The gridded hydrological model outputs, which were globally validated, might be one of the alternatives to verify the GRACE TWSC. Figure 2 shows the four sets of

TWSC derived by models in this study region. Among them, the three GLDAS hydrological models were not really independent, and generally provided consistent time-series changes, whereas large differences in magnitude still exist under dry and wet conditions (e.g., in summer and winter). There are obvious differences in phase and magnitude between GLDAS models and CPC. This may be attributed to variances in model structure, the forcing data used, and the components of the TWSC. The RMSs from Noah, VIC, Mosaic and CPC were 13 mm, 23 mm, 22 mm, and 6 mm, respectively. The average RMS was 14 mm.

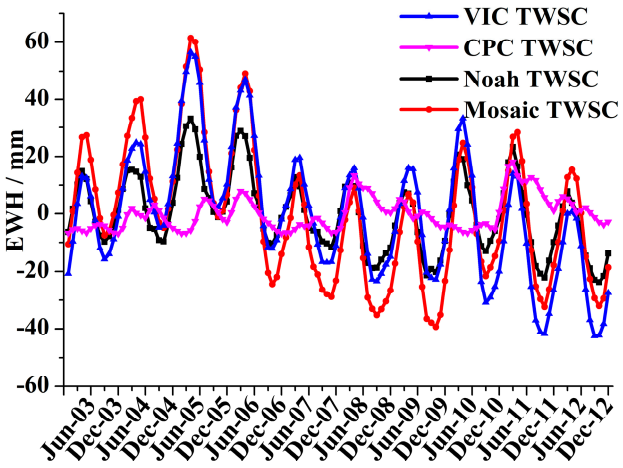


**Figure 2.** Region-averaged terrestrial water storage changes (TWSC) derived by models, Noah, VIC, Mosaic and CPC.

### *2.4. Meteorological Data*

In the ecologically fragile arid land of northwestern China, surface and ground water resources are scarce. Precipitation is the primary water source for local agriculture; therefore, precipitation has a significant influence on the local agricultural and ecological development. In this study, the relationships between TWSC, TSDI, and meteorological factors, including precipitation and air temperature, were examined. Daily precipitation and air temperature data were provided by the National Climate Centre of China Meteorological Administration. There were a total of 102 weather stations inside and around the study region (see Figure 1), with data spanning between 2003 and 2012.

The daily station data was interpolated by the Meteorological Distribution System for High-Resolution Terrestrial Modeling (MicroMet) [26] which, as a quasi-physically based and high-resolution meteorological model considering topographic effects to meteorological variables, could effectively perform spatial interpolation for variables as precipitation and air temperature. In this paper, the SRTM 90-m DEM was resampled to 10 km to drive the MicroMet model.

The Barnes objective analysis scheme and corrections were used in MicroMet to interpolate precipitation and air temperature. The reference gridded values were obtained using the Barnes objective analysis scheme with observed records and elevations. Then, a set of adjustment factors was used to calculate the final gridded precipitation/air temperature considering elevation effects, following Equations (1) and (2), respectively.

$$P = P_0 \left[ \frac{1 + \chi(z - z_0)}{1 - \chi(z - z_0)} \right] \quad (1)$$

Here, $P$ is the final interpolated precipitation (mm), $P_0$ is the reference precipitation (mm) at the station whose elevation is $z_0$ (m), $z$ the elevation (m) at the grid to be interpolated, and $\chi$ ($km^{-1}$) is the precipitation adjustment factor.

$$T = T_0 - \Gamma[z - z_0] \quad (2)$$

$T_0$ is the reference air temperature (°C) at the reference elevation of $z_0$ (m), $T$ is the final interpolated air temperature (°C) at the elevation of $z$ (m), and $\Gamma$ (°C·$km^{-1}$) is the lapse rate of air temperature.

The precipitation-elevation adjustment factors ($\chi$ in Equations (1) and (3)) and air temperature lapse rate ($\Gamma$ in Equation (2)) vary seasonally and geographically. The default monthly air temperature lapse rates ($\Gamma$ in Equation (2)) were calculated by Kunkel [27], which were generally appropriate in the Northern Hemisphere and also used in this paper. Nevertheless, the adjustment factors for precipitation were calculated following Equation (3) with monthly station precipitations and elevations at 102 meteorological stations for the period between 2003 and 2012. Then, weighted least-squares regression was used to obtain monthly adjustment factors.

$$\frac{P_1 - P_2}{P_1 + P_2} = \chi(z_1 - z_2) \quad (3)$$

Here, $P$ and $z$ are the precipitation and elevation at the station, and the subscripts represent individual stations. The monthly precipitation adjustment factors in the study area are presented in Table 1.

**Table 1.** Monthly precipitation-adjustment factors in the arid land of northwestern China.

| **Month** | **January** | **February** | **March** | **April** | **May** | **June** |
|---|---|---|---|---|---|---|
| $\chi$ ($km^{-1}$) | 0.000 | 0.000 | 0.000 | 0.015 | 0.103 | 0.150 |
| **Month** | **July** | **August** | **September** | **October** | **November** | **December** |
| $\chi$ ($km^{-1}$) | 0.169 | 0.189 | 0.177 | 0.025 | 0.000 | 0.000 |

### *2.5. Total Storage Deficit Index*

As drought brings countless problems on human societies [28], it is necessary to take effective measures to monitor the spatial scope, duration, and intensity of these phenomena so that mitigation plans can be made against the adverse effects. There are many drought-related indexes, including the Parmer Drought Severity Index (PDSI) [29], the Soil Moisture Deficit Index (SMDI) [30], the Standardized Precipitation Index (SPI) [31], and the Surface Water Supply Index (SWSI) [32] to characterize different types of drought-related disasters. These indicators have their own strengths and limitations. The PDSI is widely used and applicable for long-term weather conditions that are abnormally dry and wet. It requires inputs such as precipitation, air temperature, and other local hydrological quantities. The SMDI, usually monitoring agricultural drought, is advantageous in high temporal and spatial resolution, but is frequently restricted in use by the absence of high quality soil moisture data. The SPI has its own merit in its easy computation but it does not take into account the temperature anomalies that are also critical for drought monitoring. The SWSI, which is calculated from precipitation and from the characteristics of a variety of surface water sources (reservoir storage, snow water and stream flow), is primarily applied to the areas where precipitation is not the sole water source.

In this paper, we used TSDI, which was introduced by Yirdaw [12] and can be calculated from GRACE-derived TWSC, to create a pictorial representation of long-term dryness and wetness. The

computation of TSDI included the computation of cumulative monthly total storage deficits in the dry periods, and the determination of a drought monograph. The TSDI appeared to be more consistent with PDSI [33], which is popularly employed in drought assessment.

The monthly total storage deficit (TSD) in the study area was expressed mathematically as in Equation (4) by using the mean, maximum, and minimum water storage anomalies of each month (January to December) during the 10 years in the study period (2003–2012).

$$TSD_{i,j} = \frac{TSA_{i,j} - MTSA_j}{MaxTSA_j - MinTSA_j} \times 100 \quad (4)$$

Here, $TSD_{i,j}$ is the total storage deficit (%) of the $j$th month of the $i$th year, $TSA_{i,j}$ is the monthly total water storage anomaly (mm) derived from GRACE data, $MTSA_j$ is the mean total storage anomaly for the $j$th month (mm), $MaxTSA_j$ is the long-term maximum total storage anomaly (mm) for the $j$th month, and $MinTSA_j$ is the long-term minimum total storage anomaly for the $j$th month (mm). In this study, $i$ ranged from 2003 to 2012 and $j$ from January to December. The TSD could therefore be comparable across seasons. Depending on its value in the range between −100 and 100, the TSD was able to indicate the conditions from very dry to very wet. Drought might occur if the state of dryness continued for a prolonged period of time, thus affecting crop growth and other human activities.

Generally, a drought will gradually disappear if the dry conditions cease to be present in the following months. Thus, the TSDI was established by considering the previous drought status and the current condition of total storage deficit as given in Equation (5) [12].

$$TSDI_i = p \times TSDI_{i-1} + q \times TSD_i \quad (5)$$

Parameters $p$ and $q$ are determined as per the cumulative TSD plot during the drought period using Equation (6).

$$p = 1 - \frac{m}{m+b} \quad q = \frac{C}{m+b} \quad (6)$$

Here, $m$ indicates the slope and $b$ the intercept, both obtained from the cumulative TSD curve. The parameter $C$ stands for the intensity of the dryness condition (drought monograph) which can be retrieved from the best-fit line of the cumulative TSD during the dryness period. Palmer defined four drought classifications, and assigned corresponding values to parameter $C$: −4.0 for extreme drought, −3.0 for severe drought, −2.0 for moderate drought, and −1.0 for mild drought [33]. However, it should also be pointed out there are no uniform criteria to define the drought monograph [33]. In this study, $C$ was calculated following the method introduced by Palmer [33] and Yirdaw [12], where the parameter was determined by the cumulative TSD in conjunction with SPI, the latter being calculated from site precipitation records in and around the study area.

Developed by McKee *et al.* [31], the SPI was widely used for detecting both dry and wet conditions. Mathematically, and in accordance with the cumulative probability of a given rainfall event occurring at a station, the SPI can be determined for multiple time scales (1, 3, 6, 9, 12, 24, 48 months). A long-term precipitation record (at least 30 years) for a station was first fitted to a Gamma probability density function and then transformed into a cumulative probability function. The SPI was a random probability index with zero mean and with a variance equal to that of this probability distribution.

$$SPI = W - \frac{C_0 + C_1 W + C_2 W^2}{1 - d_1 W + d_2 W^2 + d_3 W^3}, \quad W = \begin{cases} \sqrt{-2\ln P} & for\ P \le 0.5 \\ \sqrt{-2\ln(1-P)} & for\ P > 0.5 \end{cases} \tag{7}$$

$P$ is the probability of exceeding a threshold and can be calculated following the literature [1]. The other parameters, $C_0$, $C_1$, $C_2$, $d_1$, $d_2$, and $d_3$ are constants, taking the values of 2.515517, 0.802853, 0.010328, 1.432788, 0.189269 and 0.001308 [1], respectively.

The SPI has a negative value for drought, and a positive one for wet conditions. As the dry or wet conditions become more severe, the index becomes more negative or more positive. The drought classification, based on the SPI, is shown in Table 2 [31].

**Table 2.** Drought classification based on Standardized Precipitation Index (SPI).

| Class | SPI |
|---|---|
| **Mild drought** | −1.0 < SPI ≤ −0.5 |
| **Moderate drought** | −1.5 < SPI ≤ −1.0 |
| **Severe drought** | −2.0 < SPI ≤ −1.5 |
| **Extreme drought** | SPI ≤ −2.0 |

## 3. Results

### *3.1. GRACE-Recovered TWSC*

Using GRACE satellite data, the TWSC over the arid land of northwestern China were obtained from 2003 to 2012. Prior to calculating the TSDI index, the GRACE TWSC need to be validated to ensure their accuracy within the target region. In this paper, the GRACE TWSC were compared with hydrological models TWSC and precipitation.

Figure 3 depicts the comparison between the monthly GRACE-derived and hydrological model-derived TWSC time series. Note that the model-derived TWSC were the result of averaging outputs of four hydrological models. GRACE TWSC varied from −35 to 33 mm, whereas model TWSC varied from −25 to 36 mm. The monthly TWSC from both sources showed obvious seasonal variations and agreed relatively well, with peaks in summer (June to August) and valleys in winter (December to February). As there were no surface and ground water components in the model-derived TWSC, the differences in amplitude could be discerned when compared with the GRACE TWSC. In the study region, surface and ground water was recharged mainly in the wet period, in temporal agreement with the changes in soil moisture. As a result, the two source TWSC agreed in trend but differed in amplitude as illustrated in Figure 3, where significant terrestrial water storage losses occurred between 2008 and 2009, and have been restored since 2010.

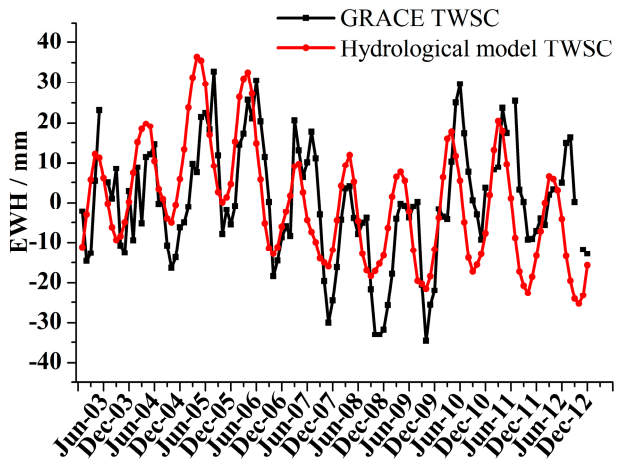


**Figure 3.** Comparison between terrestrial water storage changes (TWSC) derived by GRACE and hydrological models.

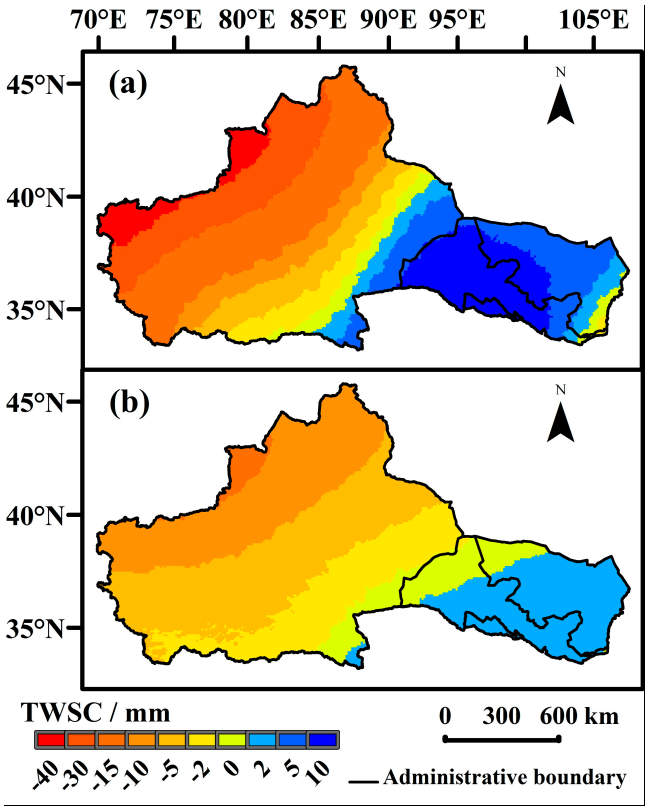


**Figure 4.** Spatial patterns of monthly averaged TWSC during 2008 and 2009. (**a**) GRACE; (**b**) hydrological models.

We also mapped the corresponding spatial patterns of TWSC by aggregating monthly TWSC during 2008 and 2009, as shown in Figure 4. The spatial distributions agreed well with each other (Figure 4a,b) with similar significant losses in the northwestern part of the study region during the two years. However, the GRACE results (Figure 4a) showed a maximum loss of around 47 mm/month, while the model results (Figure 4b) showed a maximum of only 16 mm/month. The underestimation can be attributed to incomplete TWSC components in the model estimation. The GRACE method was able to detect the total water storage changes, including groundwater and surface water, both of which were not taken into

account by the hydrological modeling method. The groundwater and surface water in the northwestern part of the study region was depleted in those years, and it accounted for about two thirds of the total water storage changes derived by GRACE. In opposition, groundwater and surface water in the east region was recharged during 2008 and 2009. Moreover, the errors in GRACE recovery and models also led to the differences in amplitude between them.

Precipitation anomalies were calculated by removing the mean of the period of January 2003 and December 2012 from every monthly precipitation value. Monthly GRACE TWSC and precipitation anomalies are shown in Figure 5a, which revealed a relatively good agreement between them, with a correlation coefficient of 0.51. The maximum synchronously appeared around June to August and the minimum around November to next January. GRACE TWSC and precipitation anomalies both showed similar periodic change trends throughout the study period. Most amounts of water were accumulated during the wet season (May–September) while they were mostly lost during the dry season (October–April).

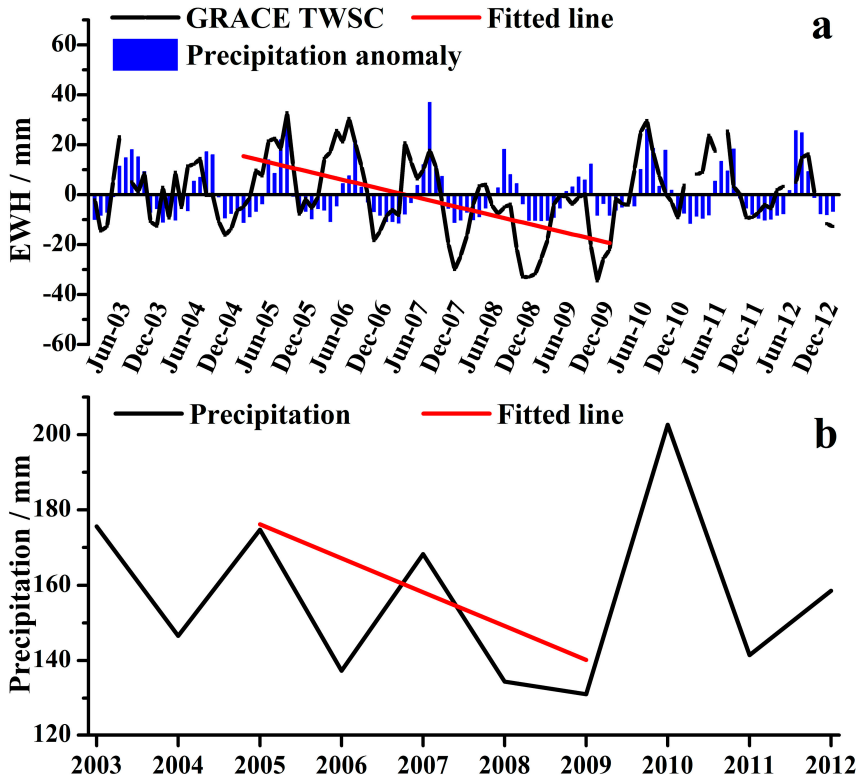


**Figure 5.** GRACE-derived TWSC and precipitation: (**a**) GRACE-derived TWSC and precipitation anomalies; (**b**) yearly annual precipitation.

For the entire study period, GRACE TWSC decreased slightly. However, a significant decline in TWSC was found between 2005 and 2009, with a trend of −0.59 mm/month. The red solid line in Figure 5a represents the best linear fit to the GRACE TWSC in the period of 2005–2009. In particular, water storage was remarkably reduced in many months during 2008–2009, even in the wet season, which contributed to the non-seasonal variability. The annual precipitation in the same period is displayed in Figure 5b. In those 10 years, annual precipitation changed year by year. The best linear fit line for the annual precipitation was also obtained for the period of 2005–2009, which shows the same obvious

decline as the GRACE TWSC. While the annual average precipitation in the arid land of northwestern China was less than 200 mm [34], annual precipitation in 2008 and 2009 was far below the average (~130 mm), while in 2010 it came back to the average (~200 mm). Along with the increase in precipitation, TWSC increased between 2010 and 2012. As shown in Figure 5b, precipitation in 2006 was about 137 mm, far below the average. However, the total water storage in the study region increased during many months in 2006 (Figure 5a). Even more than precipitation, evapotranspiration and runoff were both critical in regional water allocations. Moreover, snow/ice melt water were also crucial to supply the local water storage in the arid area of northwest China. Despite less precipitation, the joint effects of those factors increased the total water storage in 2006. Overall, the figures showed a good agreement between GRACE TWSC and precipitation, which could be explained in terms of the precipitation controlling the water storage in the arid lands. Although we lacked TWS observations as well as evapotranspiration and runoff data, the indirect comparisons support the capability of GRACE data in detecting trend changes, seasonal, and extra non-seasonal variations of TWSC in arid lands.

The high correlations observed between GRACE TWSC and hydrological model-derived TWSC, and between GRACE TWSC and precipitation, confirm that TWSC estimated by GRACE are reliable and can be used for further calculations of drought intensity and its characteristics.

### *3.2. Drought Events Detected by GRACE TSDI*

#### 3.2.1. Temporal Drought Characteristics

Figure 5a shows that the TWSC in the study region had an obvious declining trend from 2005 to 2009, reaching the lowest in 2008 and 2009. The TSD was calculated from the GRACE-derived TWSC using Equation (4) (Figure 6). The TSD values between April 2008 and December 2009 were all negative with a minimum of −29.3%, implying that the study area was dry during this period. Because the dry conditions lasted for months, and there was not enough water to recharge the water storage of the whole region, drought might have occurred from April 2008 until December 2009. The duration of dry conditions was the longest throughout the 10 years. Assuming that April 2008 was the beginning of the dry conditions, TSDs between April 2008 and December 2012 were used to obtain the parameters in Equations (5) and (6). The accumulated TSDs from April 2008 to December 2012 were computed (shown in Figure 7) to obtain the critical parameters ($m$, $b$) that were used to calculate $p$ and $q$ in Equation (5). The best fit line was obtained from the plot of the cumulative TSD during the beginning time (April 2008) and the month with the maximum cumulated TSD (April 2010). The parameters $m$ and $b$ in Equation (6) were obtained by the best fit line of the cumulative TSD plot (the solid line in Figure 7), where $m$ was the slope (−17.352), and $b$ was the y-intercept (−13.459). The critical parameter $C$ in Equation (6) was obtained from the SPI which considered only precipitation across the study region.

In order to obtain the dry and wet conditions of the arid land of northwestern China from April 2008 to December 2009, by using monthly precipitation data, the SPI values were calculated separately for each meteorological station on a 6-month time scale (SPI-6) for a period of 50 years (1963–2012). Based on the SPI-6 values, approximately 95.9% of the arid land stations suffered from drought between April, 2008 and December, 2009 as shown in Figure 8. Approximately 25.8% of the stations reported conditions of extreme drought, while 33.0% of stations reported severe drought. Moderate and mild

drought was reported by 26.8% and 10.3% of the stations, respectively. Based on these percentages, we defined the drought event during April 2008 to December 2009 as a severe dry condition, with a *C* value of −3. The cumulative TSD declined gradually from −5 in April 2008 to −398 in April 2010, after which it began to increase. The best-fit line (the solid line in Figure 7, labeled "−3") of the cumulative TSD between April 2008 and April 2010 was defined as the upper limit of severe dryness in the drought monograph. Given that the horizontal line of zero in Figure 7 represents "near normal" conditions, the interval from near normal to severe dryness was divided into three equal intervals, and the body of graph above the best-fit line of the cumulative TSD was correspondingly divided by two dashed lines labeled "−1", "−2". Using an equal interval, the fourth line was obtained and labeled "−4" in the drought monograph. The three dashed lines in Figure 7 represent the upper limits of mild, moderate and extreme dryness.

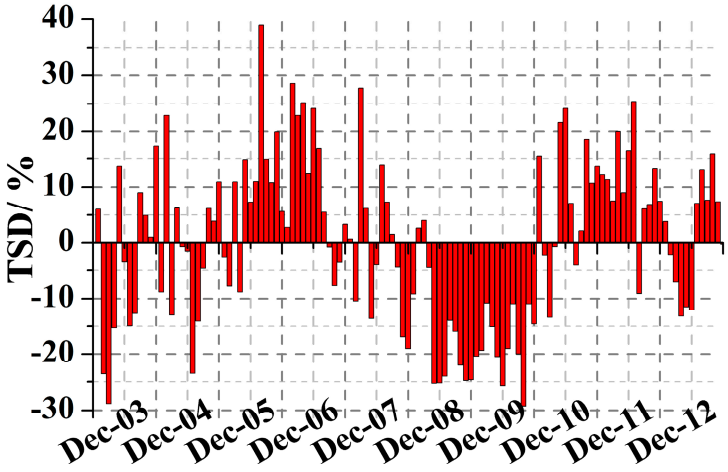


**Figure 6.** Total storage deficit (TSD, %) for the arid land during 2003–2012.

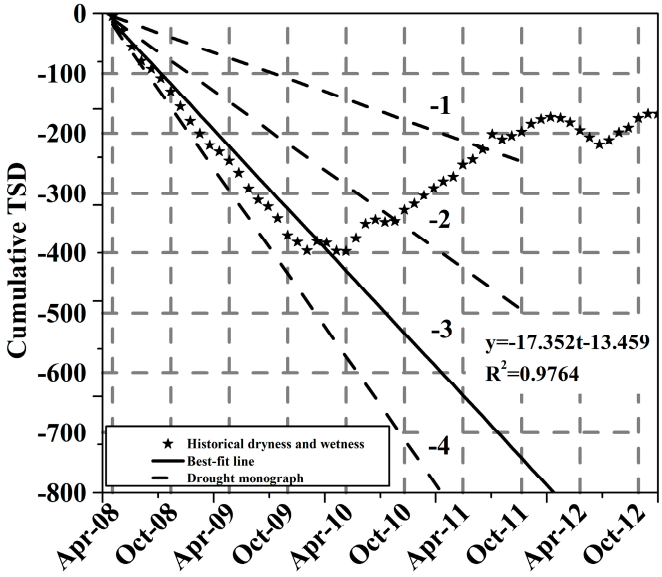


**Figure 7.** Cumulative total storage deficit (TSD) derived from GRACE TWSC for the arid land.

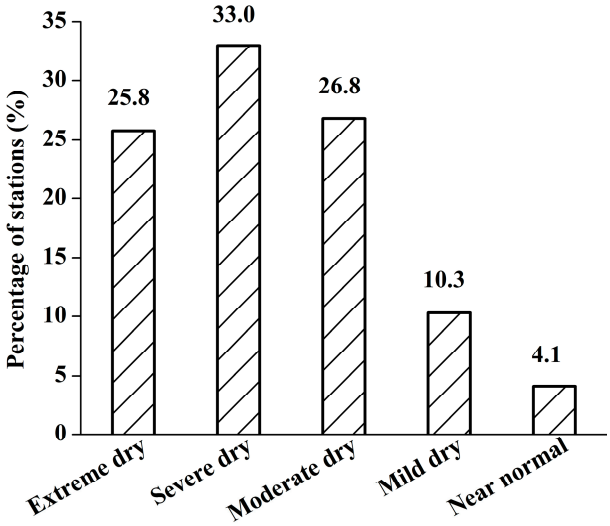


**Figure 8.** Percentage of precipitation stations on different drought severity levels from April 2008 to December 2009.

With the values of $m$ (−17.352), $b$ (−13.459), and $C$ (−3) in conjunction with Equation (6), the parameters $p$ and $q$ were determined as 0.4368 and 0.0974, respectively. By substituting the values of $p$ and $q$ into Equation (5), the monthly TSDI in the study region was calculated using Equation (8).

$$TSDI_i = 0.4368 \times TSDI_{i-1} + 0.0974 \times TSD_i \quad (8)$$

The initial TSDI, $TSDI_0$, was obtained by multiplying $TSD_1$ by a value of 2%, as described by Narasimhan and Srinivasan [30].

The distribution of TSDI over the period between 2003 and 2012 as calculated using Equation (8) is displayed in Figure 9 (blue solid line), and the drought severity classifications as per TSDI are included in Table 3.

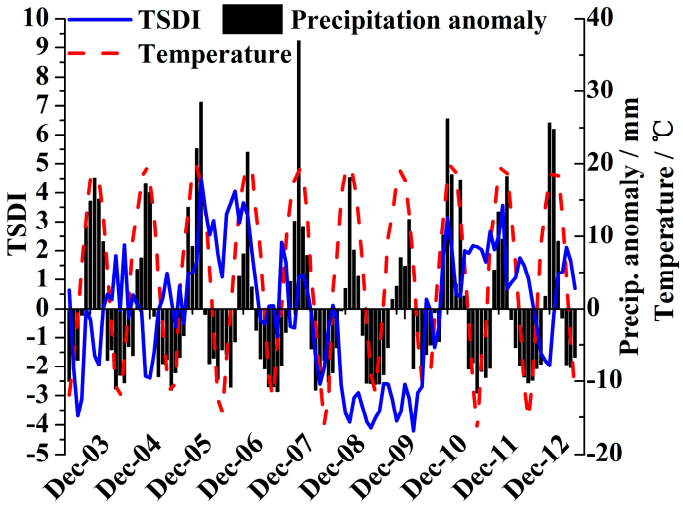


**Figure 9.** Total storage deficit index (TSDI) of the arid land.

As shown in Figure 9, the TSDI ranged from approximately −4.20–4.50 between 2003 and 2012. When the TSDI remained below −1.0 for three or more consecutive months, the period was marked as a drought event. Following this method, five droughts were identified from the GRACE data with

different durations and intensities, the latter being represented by the slope of cumulative TSDI curve in the study region (Table 4). These drought events occurred from February to April 2003, from July to September 2004, from November 2007 to January 2008, and from April to June 2012. They all had the same durations of three months, although with different intensities, indicated by varying slopes: −3.40, −1.94, −2.31 and −1.88, respectively. According to the classification table (Table 3), these drought events belonged to "severe drought", "mild drought", "moderate drought" and "mild drought", respectively. Because short-term droughts are common in arid regions, these events are not explained in detail.

**Table 3.** Drought severity classification based on TSDI.

| Class | TSDI |
|---|---|
| **Wet** | $1.0 < \text{TSDI}$ |
| **Near normal** | $-1.0 < \text{TSDI} \leq 1.0$ |
| **Mild drought** | $-2.0 < \text{TSDI} \leq -1.0$ |
| **Moderate drought** | $-3.0 < \text{TSDI} \leq -2.0$ |
| **Severe drought** | $-4.0 < \text{TSDI} \leq -3.0$ |
| **Extreme drought** | $\text{TSDI} \leq -4.0$ |

**Table 4.** Summary of GRACE TSDI-identified drought events.

| ID | Time Span | Maximum TSDI | Duration (months) | Slope of Cumulative TSDI |
|---|---|---|---|---|
| **1** | February 3 to April 3 | −3.70 | 3 | −3.40 |
| **2** | July 4 to September 4 | −2.39 | 3 | −1.94 |
| **3** | November 7 to January 8 | −2.60 | 3 | −2.31 |
| **4** | May 8 to December 9 | −4.20 | 20 | −3.35 |
| **5** | April 12 to June 12 | −1.96 | 3 | −1.88 |

Aside from the four short-term drought events, the study area experienced the longest drought event in nearly a decade between May 2008 and December 2009 (Table 4). The minimum TSDI (−4.20) was found in that time period.

The values of TSDI from May 2008 to December 2009 were totally negative, with a minimum value of −4.20 (Figure 9). The precipitation (bar) and air temperature (dash line) are also displayed in Figure 9. The changes of TSDI were a result of precipitation and air temperature anomalies. In other words, this long-term drought event was jointly caused by low precipitation and high temperature. Despite the fact that there were occurrences of positive GRACE-derived TWSC in several months between May 2008 and December 2009 (Figure 5a), these positive changes exerted no significant effects on the nearly two-year drought. Multiyear droughts could lead to the drying of surface water and soil moisture and even the loss of groundwater. The cumulative TSDI values during this drought period and their best fit line are depicted in Figure 10. The slope of the best-fit line is −3.35, indicating that this drought event belonged to the "severe drought" category. From Figure 9, it can be observed that the drought ended in December 2009 due to abundant rainfall starting in 2010 (see Figure 5).

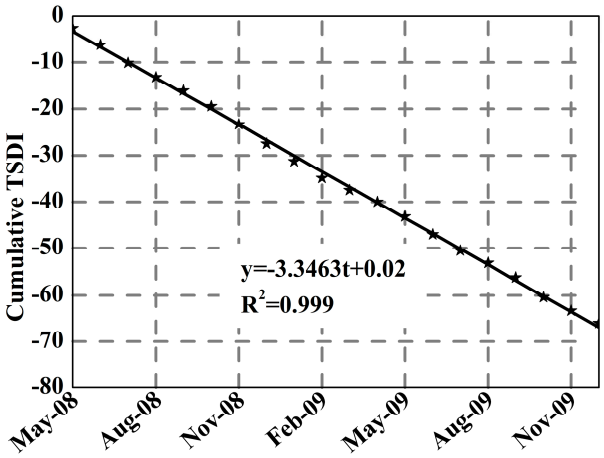


**Figure 10.** Cumulative total storage deficit index (TSDI) for the arid land of northwestern China.

3.2.2. Spatial Drought Distribution

Using Equation (4), the TSD values at the pixel scale could be obtained by gridded TWSC. Afterwards, based on Equation (8), coefficients $p$ and $q$ at the regional-scale, the gridded TSD values and the monthly spatial distribution of TSDI could be obtained. Figure 11a maps the spatial distribution of drought severity, which was represented as cumulative TSDI slope in the period of May 2008 to December 2009. As shown in Figure 11a, the drought/wet conditions over the study region spatially varied during the period. Overall, the drought intensity in Xinjiang increases spatially from southeast to northwest, and the northwest region of Xinjiang clearly suffered extreme drought. The other regions, including the Hexi Corridor, the western region of Inner Mongolia, along with southeastern parts of Xinjiang, were in near-normal or wet conditions.

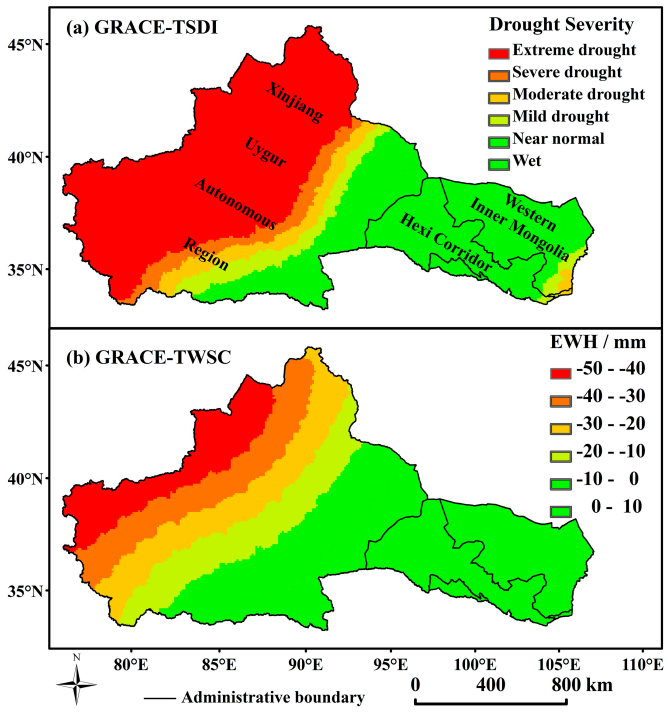


**Figure 11.** Spatial distributions of TSDI-derived drought conditions and average TWSC in the arid land of northwestern China.

The spatial distribution of averaged TWSC in the period of May 2008 to December 2009 is displayed in Figure 11b. The negative TWSC in the northwestern parts of study region indicate severe shortage of water storage, while in other regions the water storage is close to the average or slightly higher. Examining TWSC and TSDI revealed that continuing total water deficit was the primary reason to the drought disaster. Because of its location in the hinterland of the Eurasian continent, the westerly wind from the Atlantic Ocean brings a small amount of precipitation to the Xinjiang region. Drought in Xinjiang was primarily attributed to high sea level pressure, strong wind divergence, low convection of water and low water storage capacity [35]. Furthermore, the La Niña event in 2008 and 2009 also had a significant influence on the severe drought in northern China [36].

## 4. Discussion

### *4.1. Deviations with Various GRACE Data Products*

Except for the GRACE CSR data product, we also examined other data products such as GFZ and JPL. Region-averaged monthly TWSC from CSR, GFZ, and JPL are shown in Figure 12 for the study period. All TWSC results were generally consistent with each other, especially good in phase, but with variations in specific months. The trend maps were obtained by least-square fitting based on the gridded GRACE TWSC over the entire time span between 2003 and 2012. The spatial patterns of trend distributions of TWSC from CSR, GFZ, and JPL are as expected, in good agreement with each other (Figure 13a–c), although there are small deviations in some areas. The slight differences of spatio-temporal TWSC among different GRACE products are caused by the processing strategies, the tuning parameters, and the error patterns in the GRACE Science Data System [37]. Therefore, the results of this study using CSR data were independent from the selection of the GRACE data product and were able to cover the real situations in the study region.

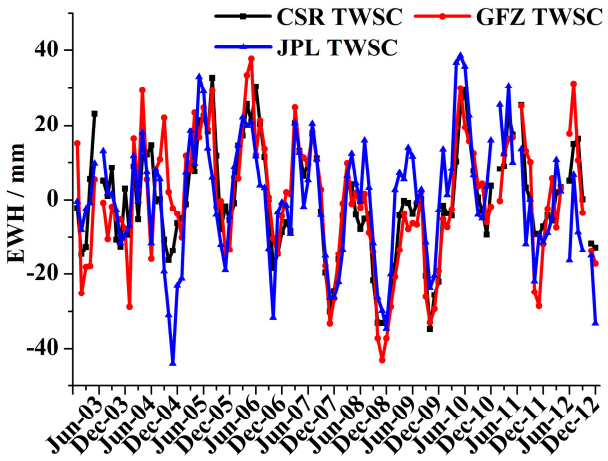


**Figure 12.** Region-averaged GRACE TWSC estimated from CSR, GFZ and JPL.

In order to further exclude possible processing errors, we tested the errors with different truncations of spherical harmonic coefficients. The degree and order of GRACE CSR RL05 solutions were up to 96, but we used a uniform truncation of 90 in this study. We tested truncations of 90 and 60 and the recovered

TWSC are shown in Figure 14. The results are pretty similar, and confirm that the errors caused by truncating to a varying degree and order, like 90 and 60, could be neglected.

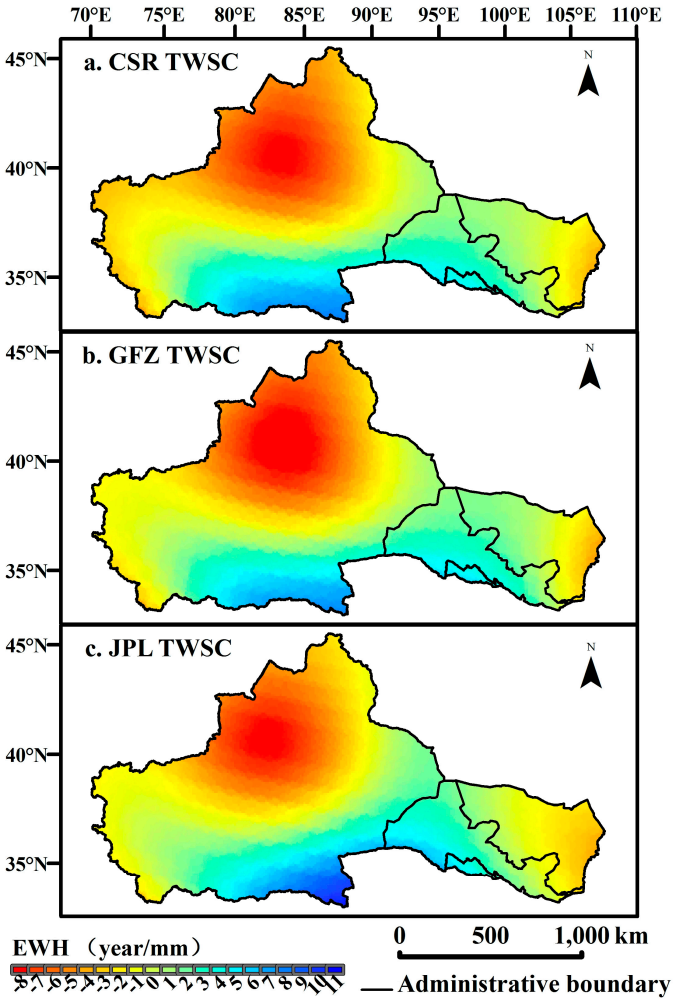


**Figure 13.** Spatial distributions of TWSC trend estimated from (**a**) CSR; (**b**) GFZ; and (**c**) JPL GRACE products.

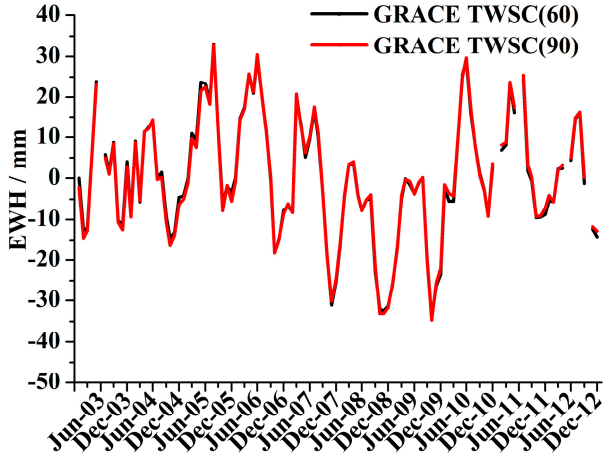


**Figure 14.** GRACE TWSC with spherical harmonic coefficients truncated to degree and order of 60 and 90.

*4.2. Uncertainties in GRACE TWSC*

Because our final calculation of the TSDI was based on the GRACE TWSC, the accuracy of GRACE TWSC determined the quality and liability of the drought index. The errors in GRACE data mainly included measurement and leakage errors. Due to the lack of *in situ* terrestrial water storage observations in the study area, it was difficult to accurately quantify the uncertainties of GRACE-derived TWSC. The measurement errors could be estimated by removing the trend, annual cycle, half annual cycle, and the 161 days of tide effect signals from the GRACE spherical harmonic coefficients [38]. The measurement errors bars, representing land residuals, following Wahr's method, are plotted in Figure 15a. Because extreme hydrological signals are not related to the long-term inter-annual variability, the measurement errors obtained by Wahr's method might be overestimated. Therefore, we used an independent method, *i.e.*, Chen's method, to re-calculate the measurement error [14]. The theory underlying this method is that the changes in ocean mass in equivalent latitudes of the study area are zero or approximately zero as the de-aliasing process for GRACE data is corrected for these changes. Therefore, residuals over the ocean could approximately represent residual errors of the study areas at equal latitudes. Following these means, the measurement errors are shown in Figure 15b. However, in view of the nature of imperfect de-aliasing process for the ocean model, the mass changes of ocean regions could be dramatic and, therefore, the measurement errors are still not ideal. Estimated measurement errors from the two methods did not differ much. They were about 10 mm of land residuals using Wahr's method and about 12 mm of ocean residuals using Chen's method. We simply averaged the two, and took their average, 11 mm, as the best estimate of measurement errors in GRACE TWSC.

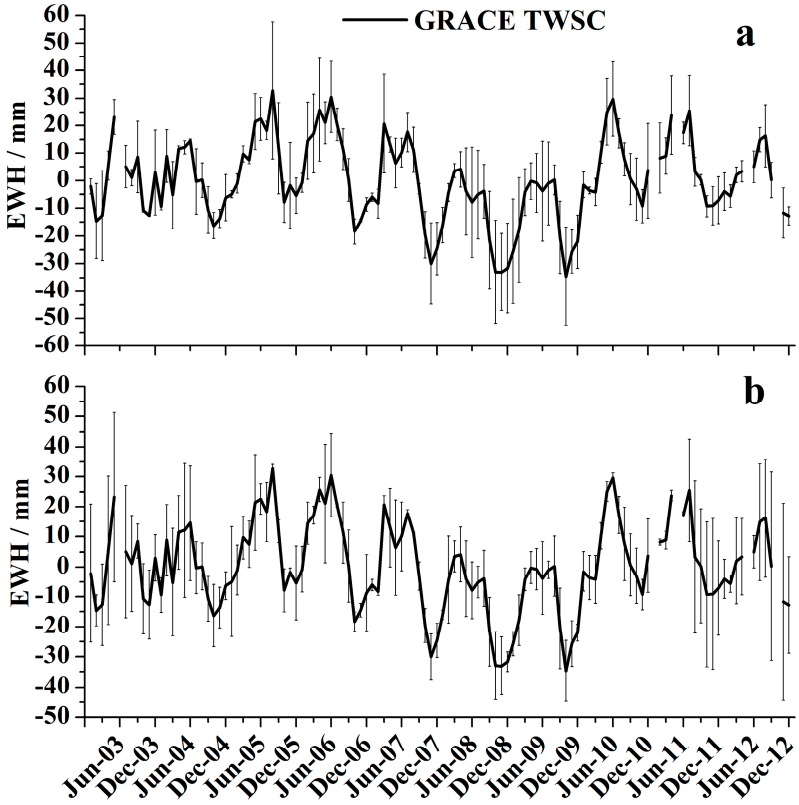


**Figure 15.** GRACE TWSC and their measurement errors: (**a**) Wahr's method; and (**b**) Chen's method.

Meanwhile, because of the use of filtering, the measurement errors were generally underestimated, as the amplitudes of both GRACE TWSC and associated errors were damped by filters. Besides, the signal attenuation, some leakage error of GRACE TWSC was also introduced by filtering and truncating GRACE spherical harmonic coefficients. A region-scale factor was used to restore the amplitude-damped GRACE TWSC and their associated errors. The region-scale factor could be computed from model based TWSC, which in this study was an average of TWSC from four models (Noah, VIC, Mosaic and CPC). The region-scale factor ($k$), expressed with Equation (9), was a result of a least-square regression by minimizing the error between the unfiltered model TWSC ($Model_{true}$) and the filtered model TWSC ($Model_{filtered}$).

$$\Delta = \sum \left( Model_{true} - kModel_{filtered} \right)^2 \tag{9}$$

Using Equation (9), we obtained a region-scale factor of 1.08. By applying the region-scale factor, the leakage error was reduced by up to 78%, being 6.3 mm rather than about 27 mm without the use of the region-scale factor. The leakage error was calculated using Equation (10) [39].

$$E_{leakage} = RMS\left( Model_{true} - kModel_{filtered} \right) \frac{RMS_{GRACE(filtered)}}{RMS_{model(filtered)}} \tag{10}$$

Multiplying the estimated measurement error by the region-scale factor suggested a scaled average measurement error of 12 mm. Thus, the total error of the study region was 14 mm, by summing measurement error and the leakage error in quadrature. The low region-mean error was attributed to the more accurate GRACE RL05 product data and to a large area of the study region, which covers a total of 2.2 million km$^2$.

### *4.3. Evaluation of TSDI Drought Detection*

Impacted by global warming, severe drought disasters over the past 30 years had occurred more frequently and with longer durations in China [8]. It was reported by Chinese Arid Meteorology that most parts of Northwest China suffered drought disasters under continuous high temperature and reduced precipitation since the summer of 2008 [40]. The longest drought from May 2008 to December 2009 was clearly observed by GRACE TSDI, with a lowest TSDI in this period. In 2008, Xinjiang suffered a drought disaster which was second in severity in record (the most severe was in 1974) [41], while the drought in the northwestern part of Xinjiang was much more severe than that in 1974 [42]. Those spatial patterns were in coincident with that detected by GRACE TSDI.

Experts have concluded that long-term high-air temperature and low levels of precipitation in mountains are the causes to the severe drought disaster in Xinjiang in 2008. In March and July 2008, the precipitation dropped by over 30% compared to other years, while the air temperature rose by 1 °C ~ 4 °C above the multiple year average, exceeding 37 °C in a number of consecutive days during May and September 2008 [43] and even up to 40 °C in some regions. A large area of crops and 47.7 million acres of pasture land in Xinjiang were under severe drought [43].

The drought continued through 2009. According to the records of China Meteorological Administration, precipitation was reduced by 30%~80%, and air temperature rose by 1 °C ~2 °C above that in previous years in most parts of the study area until the end of June 2009 [44]. About one tenth

(~2.6 million acres) of the total affected crops by drought (~23.1 million acres) had no harvest in this year due to this disaster.

Overall, both spatial and temporal distributions of drought events detected by GRACE TSDI for the arid land of northwestern China were consistent with the drought news reports and drought records in the government issued bulletins of flood and drought disasters in China.

### *4.4. TSDI vs. SPI*

Because of considering important climatic factors, SPI is believed to be effective for assessing drought severity, especially in arid regions [45]. The SPI is able to detect precipitation deficit for many time scales. Due to quick soil moisture changes in response to precipitation changes, while changes of stream flow, groundwater, and reservoir storage probably reflecting long-term changes, we further examined 3-month and 12-month SPI (Figure 16a), apart from the TSDI (Figure 16b) which used information from 6-month SPI as described in previous section. SPI-3 could represent a short time window impact to agricultural drought detection and SPI-12 represented a long time window impact to hydrological drought. The input station precipitation records were regional means from the MicroMet interpolated results from 102 sites in the period from 1963 to 2012.

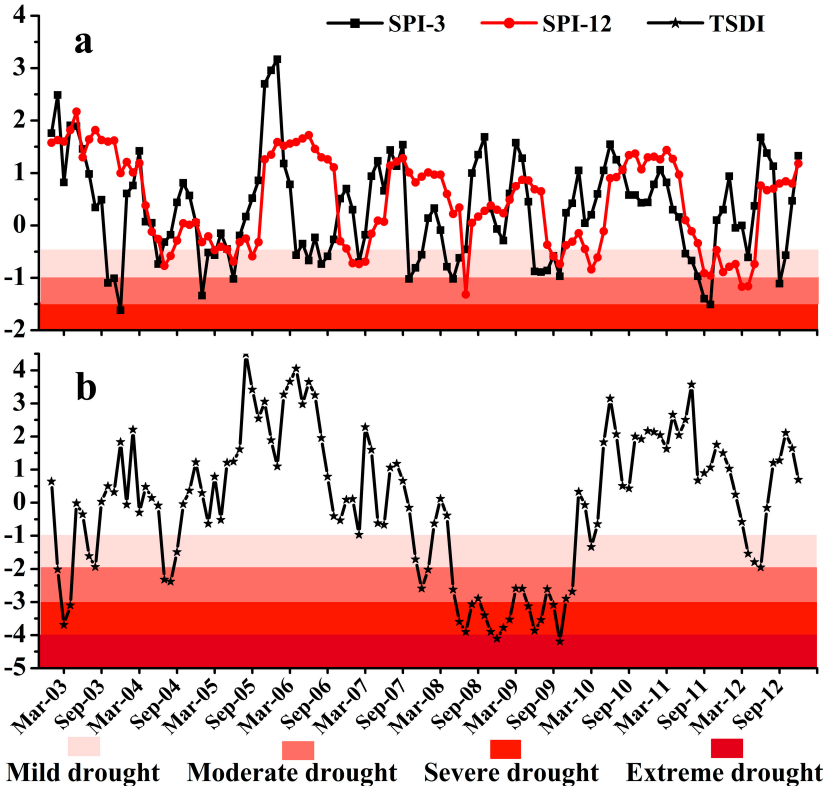


**Figure 16.** TSDI, SPI-3, and SPI-12.

Figure 16 shows the short time window SPI-3 which detected two mild drought events during the summer of 2004 and between October and December 2007, both of which were also detected by GRACE TSDI. However, there were some discrepancies between TSDI and SPI-3 derived drought events. For example, from April to June 2008 and from June to October 2009, short-term mild droughts were detected by SPI-3, although drought captured by TSDI was severe and lasted longer (Figure 16).

The one-year time window SPI-12 showed a moderate drought event in July 2008 and a mild drought event during September and October 2009, both of which were classified as severe by TSDI. In the government issued bulletins of flood and drought disasters in China in the years of 2008 and 2009 [43,44], the northwest China had suffered drought disasters in many other months during 2008 and 2009, all of which were also successfully detected by GRACE TSDI but failed to be detected by SPI-3 and SPI-12. Furthermore, a below-average drought disaster in 2011 [46] was wrongly reported as a mild drought during summer, and a moderate drought in fall detected by SPI-3 was classified as mild in fall/winter by SPI-12. However, there were actually no drought disasters in summer/fall/winter 2011 across most parts of the Northwest China [46]. Basically, SPI-3 and SPI-12 detected more mild and moderate drought events than TSDI, and missed some others such as the ones in spring 2003 and spring 2012. Those problems were not observed in the TSDI detection. Since some discrepancies exist between the TSDI and the SPI drought index, the overall agreement of TSDI with records has proven that the TSDI is a reliable integrated index in monitoring agricultural drought (3-month SPI) as well as hydrological drought (12-month SPI) over the arid land of northwestern China.

Furthermore, we should pay attention to the importance of appropriate time windows used in calculating SPI. With a short time window, SPI mainly emphasized the soil moisture changes and ignored the changes from other components. Oppositely, a long time window SPI would miss the information of short time changes. Most importantly, in the areas such as the study region, the changes of precipitation were not equal to drought conditions. Snow/glacier melt water, as another critical water sources, jointly affected water recharge in the arid land of northwestern China [15]. Especially in spring, the snow/glacier melt became a major water source for surface and subsurface water. In some circumstances, no drought occurred, with scarce precipitation but adequate glacier/snow water in the arid land. GRACE TSDI appeared to be more complete as it took into account all components of terrestrial water storage. The significant advantage of GRACE TSDI is that it considers drought conditions in a holistic manner, not only in terms of soil moisture content, but also in terms of subsurface water storage, which are usually absent in other drought indices. In western China, over-exploitation of groundwater also contributed to an increasing frequency of drought occurrences. In addition, in some mountainous areas of the study region, such as the Tianshan, the Kunlun, the Altai, and the Qilian Mountains, glacier and snow melting significantly impacted the local water balance. More glacier ablation was subject to changes in global climate [47]. Those changes, excluding precipitation changes, could not be captured by any SPI. However, they could be reflected by GRACE TSDI. For example, GRACE TSDI detected a large loss of water storage around the Tianshan Mountain, which was caused by increasing glacier ablation [48]. However, the water storage over the Xinjiang region was not alleviated under increasing runoff because human water consumption was much more excessive than before [49]. For example, approximately 86% of the total water storage was used for agriculture in the Shiyang River basin [50], which was part of the arid land of northwestern China. Moreover, GRACE TSDI, as a drought monitoring method, works on a region scale, while most traditional ones, like SPI, are based on a single point and are not fully representative on a large regional scale especially in large and terrain-complex areas.

Drought severity not only relies on climate anomalies (low rainfall and high temperature), but is also closely associated to terrestrial hydrological conditions. Taking it into account that GRACE TSDI includes all the vertical water components, it is theoretically more effective than SPI. Hence, GRACE

TSDI, based on globally covered remote sensing data, has wide application potentials, especially in the regions with scarce hydro-meteorological sites where it is impossible to support traditional methods which rely on rich site observations.

### *4.5. Forecasting Issues*

GRACE data products have latencies of two to six months and the establishment of TSDI also requires long-term data. An operational drought monitoring system may need real time or near real time inputs from GRACE data centers. In order to perform forecasting with GRACE TSDI, these issues should be addressed.

Be aware that monthly GRACE data products started from April 2002 and there was generally two to six month latencies before the data was released, which would restrict their use for drought forecasting [51]. Moreover, the follow-on GRACE mission was planned to launch in 2017 and, before this, the present GRACE satellites might stop functioning. Currently, GRACE TSDI is made on decade-long records. However, multi-decade (at least 30 years) TWSC could be more valuable in monitoring extreme hydrological events, for example. In order to carry out forecasting tasks, some methods have already been developed to extend the current available GRACE data into a longer time period. Long *et al.* [52] hindcast TWSC for a large karst plateau in Southwest China over the past three decades, by developing an artificial neural network (ANN) model to reconstruct GRACE series in combination with *in situ* precipitation, monthly mean temperature, and GLDAS soil moisture. Both the frequency and severity of droughts and floods were then obtained through the reconstructed TWSC in the last three decades. Similarly, Sun *et al.* [53] predicted groundwater table changes by using GRACE and the ANN model. De Linage *et al.* [54] proposed a simple statistical modeling framework to forecast TWSC in the Amazon Basin based on the relationship between TWSC and the sea surface temperature anomalies. However, those studies are still at preliminary stages and more efforts are required in developing the inputs to achieve sound forecasting.

## 5. Conclusions

This study investigates the spatiotemporal performances of drought monitoring using the Gravity Recovery and Climate Experiment (GRACE) gravity satellite and provides theoretical foundation for the use of a remote sensing approach in monitoring drought in the regions where only scarce data or even no data is available. Using the GRACE-derived drought indicator, the total storage deficit index (TSDI), which was calculated from the verified GRACE-recovered terrestrial water storage changes (TWSC), we monitored the drought patterns in the arid land of northwestern China, a typical large and data-scare region in China. Research results showed that GRACE-recovered TWSC was able to represent the TWSC characteristics, by comparing with hydrological model estimation and precipitation. The GRACE-derived TSDI discovered a long-term and severe drought from May 2008 to December 2009 in the study area, in addition to four short-term drought events. Spatially, the northwest Xinjiang experienced extreme drought during May 2008 and December 2009, which was caused by strong depletion in terrestrial water storage (TWS). The results were consistent with independent new reports and previous studies. A comparative analysis between GRACE-derived TSDI and traditional index confirmed a better capability of GRACE-derived TSDI in detecting drought than the traditional SPI

methods, because the former took into account all water components, rather than a single component such as precipitation like what SPI did.

GRACE-derived TSDI is the sole integrated drought indictor that considers all hydrological components for regional-to-global coverage. Our use of GRACE-derived TSDI sets up an example study of efficient drought monitoring that takes advantage of the strengths of both remote sensing and GRACE-recovered TWSC to meet the challenges of difficult access and adverse environmental conditions whereby there was sparse *in situ* data such as soil moisture and multiple year rainfall. The obtained results can be helpful for improving water resources management in Northwest China. Further research will focus on a wider application of GRACE-derived TSDI in various regions with different climatic characteristics, and then explore the applicability of an operational drought monitoring and warning program in collaboration with local meteorological departments.

## Acknowledgments

The authors would like to thank all anonymous reviewers and editors for their invaluable comments, and Shugong Wang from NASA and Felipe Hernández from University of Pittsburgh for language improvement. This study was financially supported by the NSFC/China (No. 91125006, 41471059) and IAM grant (No. IAM201215).

## Author Contributions

All authors contributed to the scientific content and authorship of this manuscript.

## Conflicts of Interest

The authors declare no conflict of interest.

## References

1. Vicente-Serrano, S.M. Differences in spatial patterns of drought on different time scales: An analysis of the Iberian Peninsula. *Water Resour. Manag.* **2006**, *20*, 37–60.
2. Mishra, A.K.; Singh, V.P. A review of drought concepts. *J. Hydrol.* **2010**, *391*, 202–216.
3. Xiao, J.F.; Zhuang, Q.L.; Liang, E.; Shao, X.M.; McGuire, A.D.; Moody, A.; Kicklighter, D.W.; Melillo, J.M. Twentieth-Century droughts and their impacts on terrestrial carbon cycling in China. *Earth Interact.* **2009**, *13*, 1–31.
4. Ministry of Water Resources (MWR). Drought disasters. In *Bulletin of Flood and Drought Disasters in China 2010*; China Water Power Press: Beijing, China, 2010; pp. 1–43.
5. Ministry of Civil Affairs (MCA). National accounts. In *China Civil Affairs Statistical Yearbook 2010*; China Statistical Press: Beijing, China, 2010; pp. 1–48.
6. Zhou, G.S.; Wang, Y.H. Global change and climate-vegetation classification. *Chin. Sci. Bull.* **2000**, *45*, 577–585.
7. Wang, H.J.; Chen, Y.N.; Chen, Z.S. Spatial distribution and temporal trends of mean precipitation and extremes in the arid region, northwest of China, during 1960–2010. *Hydrol. Process.* **2013**, *27*, 1807–1818.

8. Yu, M.X.; Li, Q.F.; Hayes, M.J.; Svoboda, M.D.; Heim, R.R. Are droughts becoming more frequent or severe in China based on the standardized precipitation evapotranspiration index: 1951–2010? *Int. J. Climatol.* **2014**, *34*, 545–558.
9. Zhai, L.X.; Feng, Q. Spatial and temporal pattern of precipitation and drought in Gansu Province, Northwest China. *Nat. Hazards* **2009**, *49*, 1–24.
10. Zhang, A.Z.; Jia, G.S. Monitoring meteorological drought in semiarid regions using multi-sensor microwave remote sensing data. *Remote Sens. Environ.* **2013**, *134*, 12–23.
11. Strassberg, G.; Scanlon, B.R.; Chambers, D. Evaluation of groundwater storage monitoring with the GRACE satellite: Case study of the High Plains aquifer, central United States. *Water Resour. Res.* **2009**, *45*, W05410.
12. Yirdaw, S.Z.; Snelgrove, K.R.; Agboma, C.O. GRACE satellite observations of terrestrial moisture changes for drought characterization in the Canadian Prairie. *J. Hydrol.* **2008**, *356*, 84–92.
13. Leblanc, M.J.; Tregoning, P.; Ramillien, G.; Tweed, S.O.; Fakes, A. Basin-scale, integrated observations of the early 21st century multiyear drought in southeast Australia. *Water Resour. Res.* **2009**, *45*, W04408.
14. Chen, J.L.; Wilson, C.R.; Tapley, B.D.; Yang, Z.L.; Niu, G.Y. 2005 drought event in the Amazon River basin as measured by GRACE and estimated by climate models. *J. Geophys. Res.* **2009**, *114*, B05404.
15. Chen, X. Research background. In *Physical Geography of Arid Land in China*; Science Press: Beijing, China, 2010; pp. 1–801.
16. Bettadpur, S. CSR Level-2, Insights into the Earth system mass variability from CSR-RL05 GRACE gravity fields. In *EGU General Assembly 2012*; EGU2012–6409; Geophysical Research Abstracts: Vienna, Austria, 2012; Volume 14.
17. Swenson, S.; Chambers, D.; Wahr, J. Estimating geocenter variations from a combination of GRACE and ocean model output. *J. Geophys. Res.* **2008**, *113*, B08410.
18. Swenson, S.; Wahr, J. Post-processing removal of correlated errors in GRACE data. *Geophys. Res. Lett.* **2006**, *33*, L08402.
19. Zhang, Z.Z.; Chao, B.F.; Lu, Y.; Hsu, H.T. An effective filtering for GRACE time-variable gravity: Fan filter. *Geophys. Res. Lett.* **2009**, *36*, L17311.
20. Paulson, A.; Zhong, S.J.; Wahr, J. Inference of mantle viscosity from GRACE and relative sea level data. *Geophys. J. Int.* **2007**, *171*, 497–508.
21. Rodell, M.; Houser, P.R.; Jambor, U.E.A.; Gottschalck, J.; Mitchell, K.; Meng, C.; Arsenault, K.; Cosgrove, B.; Radakovich, J.; Bosilovich, M. The global land data assimilation system. *Bull. Am. Meteorol. Soc.* **2004**, *85*, 381–394.
22. Rodell, M.; Chen, J.; Kato, H.; Famiglietti, J.S.; Nigro, J.; Wilson, C.R. Estimating groundwater storage changes in the Mississippi River basin (USA) using GRACE. *Hydrogeol. J.* **2007**, *15*, 159–166.
23. Syed, T.H.; Famiglietti, J.S.; Rodell, M.; Chen, J.L.; Wilson, C.R. Analysis of terrestrial water storage changes from GRACE and GLDAS. *Water Resour. Res.* **2008**, *44*, W02433.
24. Feng, W.; Zhong, M.; Lemoine, J.M.; Biancale, R.; Hsu, H.T.; Xia, J. Evaluation of groundwater depletion in North China using the Gravity Recovery and Climate Experiment (GRACE) data and ground-based measurements. *Water Resour. Res.* **2013**, *49*, 2110–2118.

25. Wang, H.S.; Wu, P.; Wang, Z.Y. An approach for spherical harmonic analysis of non-smooth data. *Comput. Geosci.* **2006**, *32*, 1654–1668.
26. Liston, G.E.; Elder, K. A meteorological distribution system for high-resolution terrestrial modeling (MicroMet). *J. Hydrometeorol.* **2006**, *7*, 217–234.
27. Kunkel, K.E. Simple procedures for extrapolation of humidity variables in the mountainous western United States. *J. Clim.* **1989**, *2*, 656–669.
28. Shewale, M.P.; Kumar, S. *Climatological Features of Drought Incidences in India*; National Climate Centre Office of the Additional Director General of Meteorology Research, Indian Meteorological Department: Pune, India, 2005; pp. 1–24.
29. Dai, A.G. Characteristics and trends in various forms of the Palmer Drought Severity Index during 1900–2008. *J. Geophys. Res.* **2011**, *116*, D12115.
30. Narasimhan, B.; Srinivasan, R. Development and evaluation of soil moisture deficit index (SMDI) and evapotranspiration deficit index (ETDI) for agricultural drought monitoring. *Agric. For. Meteorol.* **2005**, *133*, 69–88.
31. McKee, T.B.; Doesken, N.J.; Kleist, J. The relationship of drought frequency and duration to time scales. In Proceedings of the 8th Conference on Applied Climatology, Anaheim, CA, USA, 17–22 January 1993; American Meteorological Society: Boston, MA, USA, 1993; pp. 179–183.
32. Garen, D.C. Revised surface-water supply index for western United States. *J. Water Resour. Plan. Manag.* **1993**, *119*, 437–454.
33. Palmer, W.C. *Meteorological Drought*; US Department of Commerce, Weather Bureau: Washington, DC, USA, 1965.
34. Zheng, C.L.; Wang, Q. Spatiotemporal variations of reference evapotranspiration in recent five decades in the arid land of Northwestern China. *Hydrol. Process.* **2014**, *28*, 6124–6134.
35. Mahmood, R.; Li, S.L.; Khan, B. Causes of recurring drought patterns in Xinjiang, China. *J. Arid Land* **2010**, *2*, 279–285.
36. Gao, H.; Yang, S. A severe drought event in northern China in winter 2008–2009 and the possible influences of La Niña and Tibetan Plateau. *J. Geophys. Res.* **2009**, *114*, D24104.
37. Sakumura, C.; Bettadpur, S.; Bruinsma, S. Ensemble prediction and intercomparison analysis of GRACE time-variable gravity field models. *Geophys. Res. Lett.* **2014**, *41*, 1389–1397.
38. Wahr, J.; Swenson, S.; Velicogna, I. Accuracy of GRACE mass estimates. *Geophys. Res. Lett.* **2006**, *33*, L06401.
39. Landerer, F.W.; Swenson, S.C. Accuracy of scaled GRACE terrestrial water storage estimates. *Water Resour. Res.* **2012**, *48*, W04531.
40. Ministry of Environmental Protection of the People's Republic of China. Available online: http://jcs.mep.gov.cn/hjzl/zkgb/2008zkgb/200906/t20090609_152543.htm (accessed on 12 January 2015).
41. Li, L.H. The Research of Drought Monitoring for in the North of Xinjiang. Master's Thesis, Xinjiang University, Urumqi, China, 2010.
42. Tang, S.Z. Drought characteristics and countermeasures in the northern region of Xinjiang Tacheng in 2008. *China Flood Drought Manag.* **2010**, *20*, 71–74.
43. Ministry of Water Resources (MWR). Drought disasters. In *Bulletin of Flood and Drought Disasters in China 2008*; China Water Power Press: Beijing, China, 2008; pp. 1–48.

44. Ministry of Water Resources (MWR). Drought disasters. *Bulletin of Flood and Drought Disasters in China 2009*; China Water Power Press: Beijing, China, 2009; pp. 1–47.
45. Barros, A.P.; Bowden, G.J. Toward long-lead operational forecasts of drought: An experimental study in the Murray-Darling River basin. *J. Hydrol.* **2008**, *357*, 349–367.
46. Ministry of Water Resources (MWR). Drought disasters. *Bulletin of Flood and Drought Disasters in China 2011*; China Water Power Press: Beijing, China, 2011; pp. 1–47.
47. Su, Z.; Shi, Y.F. Response of monsoonal temperate glaciers to global warming since the Little Ice Age. *Quat. Int.* **2002**, *97–98*, 123–131.
48. Matsuo, K.; Heki, K. Time-variable ice loss in Asian high mountains from satellite gravimetry. *Earth Planet. Sci. Lett.* **2010**, *290*, 30–36.
49. Wang, H.J.; Chen, Y.N.; Li, W.; Deng, H. Runoff responses to climate change in arid region of northwestern China during 1960–2010. *Chin. Geogr. Sci.* **2013**, *23*, 286–300.
50. Li, Z.L.; Xu, Z.X.; Li, J.Y.; Li, Z.J. Shift trend and step changes for runoff time series in the Shiyang River basin, Northwest China. *Hydrol. Process.* **2008**, *22*, 4639–4646.
51. Famiglietti, J.S.; Rodell, M. Water in the balance. *Science* **2013**, *340*, 1300–1301.
52. Long, D.; Shen, Y.J.; Sun, A.; Hong, Y.; Longuevergne, L.; Yang, Y.T.; Li, B.; Chen, L. Drought and flood monitoring for a large karst plateau in Southwest China using extended GRACE data. *Remote Sens. Environ.* **2014**, *155*, 145–160.
53. Sun, A.Y. Predicting groundwater level changes using GRACE data. *Water Resour. Res.* **2013**, *49*, 5900–5912.
54. De Linage, C.; Famiglietti, J.S.; Randerson, J.T. Statistical prediction of terrestrial water storage changes in the Amazon basin using tropical Pacific and North Atlantic sea surface temperature anomalies. *Hydrol. Earth Syst. Sci.* **2014**, *18*, 2089–2102.